Article

Crystals in CrystalsNanocrystals within Mesoporous Zeolite Single Crystals

Claus H. Christensen, Iver Schmidt, Anna Carlsson, Kim Johannsen, and Konrad Herbst

J. Am. Chem. Soc., **2005**, 127 (22), 8098-8102• DOI: 10.1021/ja050380u • Publication Date (Web): 13 May 2005

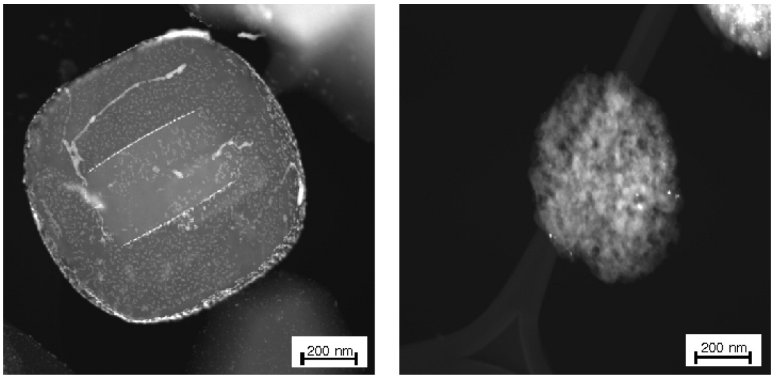

More About This Article

Additional resources and features associated with this article are available within the HTML version:

- Supporting Information
- Links to the 5 articles that cite this article, as of the time of this article download
- Access to high resolution figures
- Links to articles and content related to this article
- Copyright permission to reproduce figures and/or text from this article

View the Full Text HTML

J|A|C|S
ARTICLES
Published on Web 05/13/2005

Crystals in Crystals—Nanocrystals within Mesoporous Zeolite Single Crystals

Claus H. Christensen,[†,‡] Iver Schmidt,[†] Anna Carlsson,[†] Kim Johannsen,*[,†] and Konrad Herbst[†]

Contribution from Haldor Topsøe A/S, Nymøllevej 55, DK-2800 Lyngby, Denmark, and Center for Sustainable and Green Chemistry, Department of Chemistry, Technical University of Denmark, DK-2800 Lyngby, Denmark

Received January 20, 2005; E-mail: kjo@topsoe.dk

Abstract: A major factor governing the performance of catalytically active particles supported on a zeolite carrier is the degree of dispersion. It is shown that the introduction of noncrystallographic mesopores into zeolite single crystals (silicalite-1, ZSM-5) may increase the degree of particle dispersion. As representative examples, a metal (Pt), an alloy (PtSn), and a metal carbide (β-Mo_2C) were supported on conventional and mesoporous zeolite carriers, respectively, and the degree of particle dispersion was compared by TEM imaging. On conventional zeolites, the supported material aggregated on the outer surface of the zeolite particles, particularly after thermal treatment. When using mesoporous zeolites, the particles were evenly distributed throughout the mesopore system of the zeolitic support, even after calcination, leading to nanocrystals within mesoporous zeolite single crystals.

Introduction

Zeolites are naturally occurring or artifically created compounds consisting of tetrahedral SiO_4 units linked together in intricate crystalline frameworks. These frameworks contain crystallographically determined micropores with diameters between 3 and 10 Å, giving the zeolite molecular-sieving capabilities. By now more than 145 types of zeolites, each with a unique crystalline structure and micropore system, have been identified.[1]

Zeolites can be chemically modified in a number of ways, of which metal substitution is the most common. Different metals, most notably Al, can replace some of the Si atoms in the framework, in which case the framework acquires a negative charge for each AlO_4 unit. The negative charges are countered by cations. If this cation is H^+, the zeolite becomes acidic. In the last few decades, examples of other metals substituted into the framework have been investigated, such as Ti,[2] V[3] (giving the zeolite oxidative properties), and several other metals.

Alternatively to chemical modification of the framework, the use of zeolites as carrier material for catalytically active components such as metals, alloys, carbides, and sulfides has been investigated. The catalytic properties of these materials when supported on zeolites can be drastically different to the bulk materials due to the dispersion of these materials in the zeolite matrix. Furthermore, the acidity of the zeolite is combined with the catalytic properties of the supported component, giving rise to bifunctional catalysts.

However, if these zeolite-supported materials are to have the desired catalytic properties, two conditions have to be met:

(1) The acidic site and the supported material generally have to be in close proximity.

(2) The material has to be well-dispersed throughout the zeolite.

These conditions are often difficult to achieve, since the supported material in almost all cases remains on the outer surface of the zeolite as bulk material, while the acidic sites are dispersed throughout the zeolite single crystal.[4]

Indeed, only a few examples of supported material within the micropores are known, in which case the preparation procedure is more delicate than the usual impregnation procedures. The catalytic activity of the supported material in the micropores seems to be low, probably due to spatial restraints in the micropores.[5] Thus, there is a need to develop bifunctional zeolitic catalysts with high dispersion, in which the catalytically active component is located neither at the outer surface nor the micropore system.

One possibility is to increase the external surface area. Different techniques for production of nanosized zeolites have been developed, one example being the confined space synthesis.[6] Unfortunately, nanosized crystals exhibit problems of handling.

As an alternative, different mesoporous materials have been presented. Most notable is the M41S family of mesoporous materials,[7] but they lack the crystallinity which is seen in zeolite

[†] Haldor Topsøe A/S.
[‡] Technical University of Denmark.

(1) Database of zeolite structures: http://www.iza-structure.org/databases/.
(2) Taramasso, M.; Perego, G.; Notari, B. US Patent 4,410,501, 1983.
(3) Centi, G.; Perathoner, S.; Trifiro, F.; Aboukais, A.; Aissi, C. F.; Guelton, M. *J. Phys. Chem.* **1992**, *96*, 2617.
(4) Knapp, C.; Obuchi, A.; Uchisawa, J. O.; Kushiyama, S.; Avila, P. *Microporous Mesoporous Mater.* **1999**, *31*, 23.
(5) Hensen, E. J. M.; van Veen, J. A. R. *Catal. Today* **2003**, *86*, 87.
(6) Madsen, C.; Jacobsen, C. J. H. *Chem. Commun.* **1999**, 673.
(7) Kresge, C. T.; Leonowicz, M. E.; Roth, W. J.; Vartuli, J. C.; Beck, J. S. *Nature* **1992**, *359*, 710.

10.1021/ja050380u CCC: $30.25

Scheme 1. Principles of Synthesis Procedures for Conventional and Mesoporous Zeolites

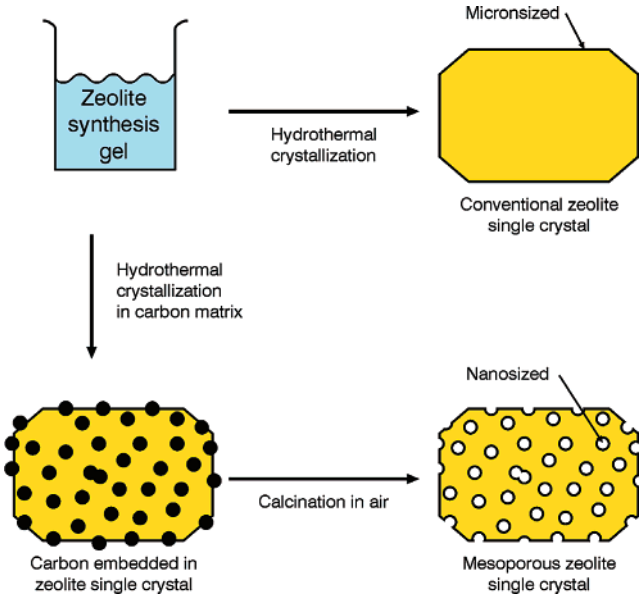

crystals, severely limiting the potential of these materials. Also, the delaminated zeolites of the ITQ-type have been presented as an example of zeolitic materials with increased surface area,[8] but they exhibit the same difficulty in handling as nanosized crystals as well as a delicate preparation procedure, which seems to limit their application.

Recently, a new family of crystalline zeolitic materials was presented, the so-called mesoporous zeolite single crystals. This new material features individual zeolite single crystals with an additional noncrystalline mesopore system interconnected with the usual micropore system of the zeolite, resulting in a bimodal pore distribution. These materials are produced by crystallizing the zeolite around a removable matrix, most often carbon (see Scheme 1). By adjusting the carbon matrix, mesopores with different pore size and tortuosity can be produced.[9,10] Other schemes have been presented as well, such as assembling zeolite seeds with organic structure directors present,[11] by resin macrotemplating,[12] or by using carbon aerogels.[13]

The introduction of this noncrystalline mesopore system leads to a number of different positive effects on the performance of mesoporous zeolites in catalysis. Two examples, which have previously been shown, are *better resistance to deactivation*,[14] which is of major importance in many industrial catalytic applications (one important example being Mo on HZSM-5 for dehydroaromatization of methane[15]) and a *significant decrease in transport limitation*.[16] Both of these factors have a marked influence on the catalytic properties, and it has been shown that

Scheme 2. Comparison of Impregnation and Thermal Activation Steps on Conventional and Mesoporous Zeolites

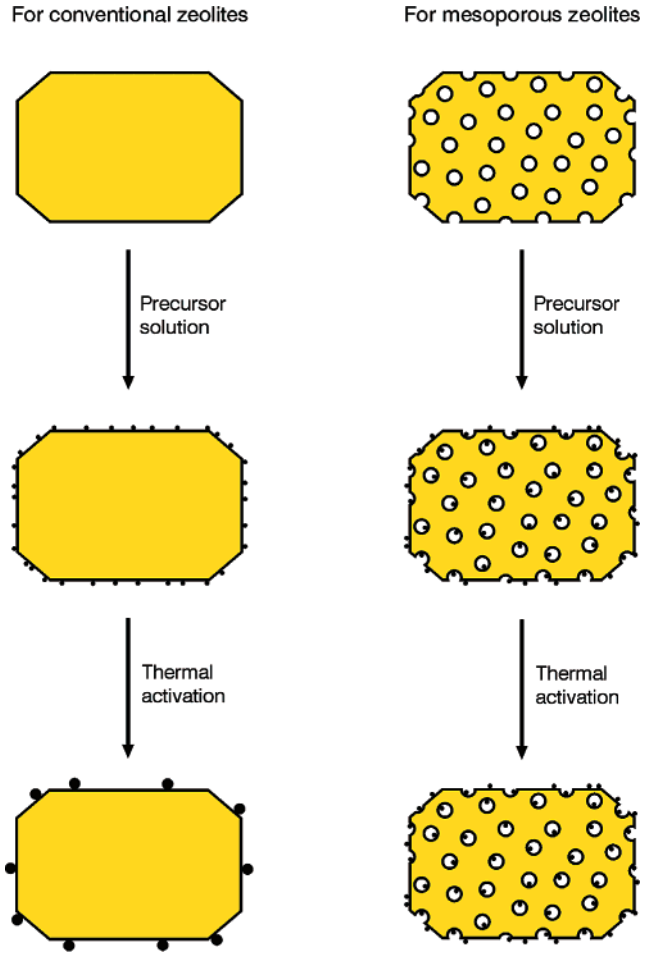

it is possible to have increased activity, selectivity, and lifetime of the catalyst in several processes.[17−19]

Thus, hierarchical zeolites such as the mesoporous zeolites are of significant interest both in materials science and catalysis. But mesoporous zeolites do not only offer advantages as pure compounds. They also seem to be suitable candidates for bifunctional catalysts.[16] The increased surface area would not only decrease transport limitations in the zeolite but also be beneficial in the effort to disperse the catalytic phase in the zeolite to a higher degree than what has been seen in conventional zeolite single crystals. This will result in smaller crystals of the supported material in closer proximity to the acidic sites than previously seen with conventional zeolites (Scheme 2).

Experimental Section

Preparation of Zeolite Materials. Conventional zeolite single crystals (silicalite-1 and H-ZSM-5) were prepared according to the literature.[20] The mesoporous zeolite single crystal samples (silicalite-1 and H-ZSM-5) were prepared as described previously using carbon

(8) Corma, A.; Fornés, V.; Martínez-Triguero, J.; Pergher, S. B. *J. Catal.* **1999**, *186*, 57.
(9) Jacobsen, C. J. H.; Madsen, C.; Houžvicka, J.; Schmidt, I.; Carlsson, A. *J. Am. Chem. Soc.* **2000**, *122*, 7116.
(10) Janssen, A. H.; Schmidt, I.; Jacobsen, C. J. H.; Koster, A. J.; De Jong, K. P. *Microporous Mesoporous Mater.* **2003**, *65*, 59.
(11) Liu, Y.; Pinnavaia, T. J. *J. Mater. Chem.* **2004**, *14*, 1099.
(12) Naydenov, V.; Tosheva, L.; Sterte, J. *Microporous Mesoporous Mater.* **2000**, *35*−*36*, 621.
(13) Tao, Y.; Kanoh, H.; Kaneko, K. *J. Phys. Chem. B* **2003**, *107*, 10974.
(14) Janssens, T. V. W.; Dahl, S.; Jacobsen, C. J. H. EP 1,479,662.
(15) Su, L.; Liu, L.; Zhuang, J.; Wang, H.; Li, Y.; Shen, W.; Xu, Y.; Bao, X. *Catal. Lett.* **2003**, *91*, 155.
(16) Hartmann, M. *Angew. Chem., Int. Ed.* **2004**, *43*, 2−4.
(17) Christensen, C. H.; Johannsen, K.; Schmidt, I.; Christensen, C. H. *J. Am. Chem. Soc.* **2003**, *125*, 13370.
(18) Schmidt, I.; Krogh, A.; Wienberg, K.; Carlsson, A.; Brorson, M.; Jacobsen, C. J. H. *Chem. Commun.* **2000**, 2157.
(19) Houžvicka, J.; Jacobsen, C. J. H.; Schmidt, I. *Stud. Surf. Sci. Catal.* **2001**, *135*, 158.
(20) Robson, H.; Lillerud, K. P. *Verified Synthesis of Zeolitic Materials*, 2nd ed.; Elsevier: Amsterdam, 2001.

black pearls (particle size 18 nm) as carbon matrix.[10,18] This results in samples with mesopore volumes in the range of 0.4−1.2 mL/g.

Preparation of Supported Samples. Three sets of supported samples were prepared, each on mesoporous and conventional zeolite.

Pt/Silicalite-1. $Pt(norbornene)_3$ (norbornene = bicyclo[2.2.1]hept-2-ene) was prepared according to the literature.[21] The Pt/silicalite-1 sample was prepared by conventional Schlenk line techniques. Zeolite silicalite-1 (3.5 g) was dried at 200 °C for 2 h and cooled to ambient temperature in N_2 atmosphere. The sample was impregnated by a solution of $Pt(norbornene)_3$ (172 mg) in CH_2Cl_2 (2.8 mL). After standing for 1 h, the solvent was evaporated in a vacuum. The evacuated sample was heated to 90 °C for 2 h to decompose $Pt(norbornene)_3$. After cooling, the sample was washed with pentane and dried in a vacuum.

Another sample on mesoporous silicalite-1 was prepared similarly by impregnation of 78 mg $Pt(norbornene)_3$ dissolved in CH_2Cl_2 (1.8 mL) on 1.6 g mesoporous silicalite-1.

Both Pt/silicalite-1 samples were calcined at 500 °C (heating ramp 1 °C/min) for 1 h with airflow over the sample.

PtSn/Silicalite-1. Both 0.36 g of $SnCl_2 \cdot 2H_2O$ and 0.24 g of H_2PtCl_6 were dissolved in 10 mL of 0.01 M hydrochloric acid, and 5.0 g of silicalite-1 was suspended in the solution with stirring for 2 h. Water was evaporated in a vacuum, and the sample was dried overnight at 110 °C. The sample was calcined in air at 400 °C for 4 h, cooled, reduced in H_2 at 400 °C for 2 h, cooled, and passivated in 3% O_2/He at room temperature for 1 h. Another sample was prepared similarly, using mesoporous silicalite-1.

***β*-Mo_2C/ZSM-5.**[22] A slurry was formed by mixing 50 g of HZSM-5 with 75 mL of distilled water. An aqueous molybdate solution to obtain a 10 wt % Mo loading was prepared by dissolving 10.7 g of ammonium heptamolybdate (Aldrich, +99.5%, AHM) in 75 mL of distilled water by gently heating to 80 °C while being stirred for 15 min. The hot AHM solution was slowly added to the zeolite slurry with stirring. Then the temperature was increased to 80 °C, whereby a yellow slurry was formed, and the water was evaporated with stirring for approximately 2 h.

The dried material was pressed into tablets, crushed, and sieved into a 250−425 μm fraction, which was loaded into a flow reactor. Calcination was carried out in a flow (1.0 NL/h) of dry air by increasing the temperature to 400 °C at a rate of 5 °C/min and keeping it there for 1 h before cooling.

After flushing the reactor with He, the preactivation feed consisting of a 1:9 *n*-butane/hydrogen mixture was introduced. Then the temperature was increased to 350 °C at 15 °C/min and kept at this temperature for 10 h. After changing the feed gas to methane, the temperature was increased to 700 °C at 5 °C/min and held for 1 h before cooling to room temperature.

Characterization. The crystal sizes of the zeolite samples were determined by conventional scanning electron microscopy (SEM) and (scanning) transmission electron microscopy (TEM/STEM), the crystallinity of the zeolites was analyzed by X-ray powder diffraction (XRPD), and the elemental composition was determined by inductively coupled plasma spectroscopy (ICP). The particle sizes of the active phases were determined by (S)TEM. It was not possible to obtain reliable data on metal dispersion using chemisorption techniques or to measure particle sizes using XRPD due to the low metal loading of the samples.

In TEM experiments, the samples were characterized using either bright field TEM or dark field STEM, depending on the nature of the sample. About 100 crystals were investigated for each sample, and representative examples are shown here. The TEM was coupled with energy dispersive spectroscopy (EDS) mapping to determine the distribution of different elements in the individual single crystals. The acquisition time for the EDS acquisition was adjusted so that clear peaks were obtained also for the low-concentration elements in the spectra.

Table 1. Metal Loading of the Samples As Determined by ICP

sample	metal load (wt %)
Pt/mesoporous silicalite-1	2.0
Pt/conventional silicalite-1	1.9
Pt/mesoporous silicalite-1, calcined	2.1
Pt/conventional silicalite-1, calcined	2.1
PtSn/mesoporous silicalite-1	1.3 (Pt), 1.1 (Sn)
PtSn/conventional silicalite-1	1.5 (Pt), 0.7 (Sn)
β-Mo_2C/mesoporous ZSM-5	10.6
β-Mo_2C/conventional ZSM-5	10.2

The EDS line scans and maps were calculated from the integrated intensities of the relevant peaks after background subtraction.

Results and Discussion

Zeolites and General Sample Characterization. All zeolite samples were 100% crystalline, as judged from XRPD. The crystal size of the two H-ZSM-5 samples were equal (1 μm), whereas the crystals of the mesoporous silicalite-1 sample were smaller (0.5 μm) than the conventional silicalite-1 crystals (2 μm). The two H-ZSM-5 samples had Si/Al ratios of 40. The metal loadings of the samples prepared on the zeolites are displayed in Table 1.

TEM confirmed that the two mesoporous samples indeed consisted of mesoporous single crystals and not agglomerates of nanosized crystals. Using TEM images it is difficult to determine the location of metal particles, since TEM images are 2D projections of 3D objects; thus, it is not straightforward to determine whether metal particles are located in the intracrystalline mesopores as well as at the geometrical external surface or exclusively on the geometrical external surface. Recently, stereo-TEM characterization of mesoporous zeolites showed that the metal particles present in the samples are located in the intracrystalline mesopores as well as the external surface of the mesoporous zeolite single crystals.[23] However, in these samples the metal was introduced unintentionally as an impurity in the carbon matrix during synthesis, and furthermore, no conclusions about the distribution between micro- and mesopores were reached. But the results in ref 23 indicate that the metal particles distributed on mesoporous zeolites in general are most likely located in the intracrystalline mesopores as well as on the external surface of the zeolite crystals.

Pt/Silicalite-1. Supported Pt catalysts are extensively used for a number of different reactions, both in research and industry.[24] Due to their excellent hydrogenating properties for several functional groups, Pt supported on Al_2O_3 or SiO_2 has found widespread application in a number of refinery processes. Large-scale applications of Pt catalysts supported on zeolite Y are also found for skeletal isomerization processes of C_4-C_8 paraffin hydrocarbon streams in refineries.

Despite the very similar Pt loadings on both the conventional and mesoporous silicalite-1 samples, significant differences of Pt distribution on the carrier particles are apparent from the TEM images with corresponding EDS line scans (Figure 1). In the conventional silicalite-1 sample (Figure 1a,c) the twinned shape of the silicalite-1 particle is recognized as an increase of the Si signal at 320 nm and a corresponding decrease at 720 nm. Pt is located as a thin layer around the outer surface of the zeolite

(21) Crascall, L. E.; Spencer, J. L. *Inorg. Synth.* **1990**, *28*, 127.
(22) Bouchy, C.; Schmidt, I.; Anderson, J. R.; Jacobsen, C. J. H.; Derouane, E. G.; Derouane-Abd Hamid, S. B. *J. Mol. Catal. A: Chem.* **2000**, *163*, 283.
(23) Boisen, A.; Schmidt, I.; Carlsson, A.; Dahl, S.; Brorson, M.; Jacobsen, C. J. H. *Chem. Commun.* **2003**, 958.
(24) Cornils, B., Herrmann, W. A., Schlögl, R., Wong, C.-H., Eds.; *Catalysis from A to Z*; Wiley-VCH: Weinheim (Germany) 2000; p 451f.

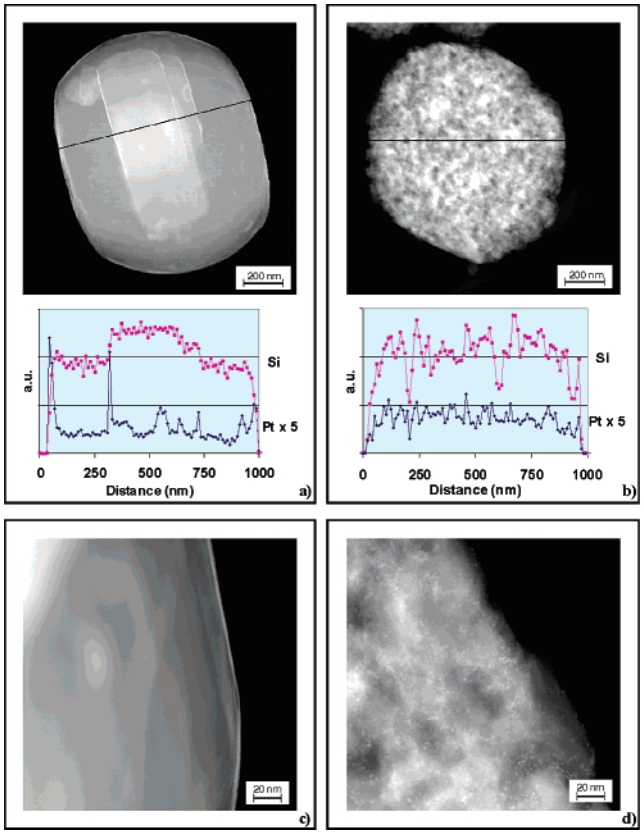

Figure 1. TEM images of Pt/conventional silicalite-1 (left column) and Pt/mesoporous silicalite-1 (right column) before calcination. Element-sensitive EDS line scans (position indicated by lines in images) giving relative atomic concentrations for Pt (bottom) and Si (top) are also shown.

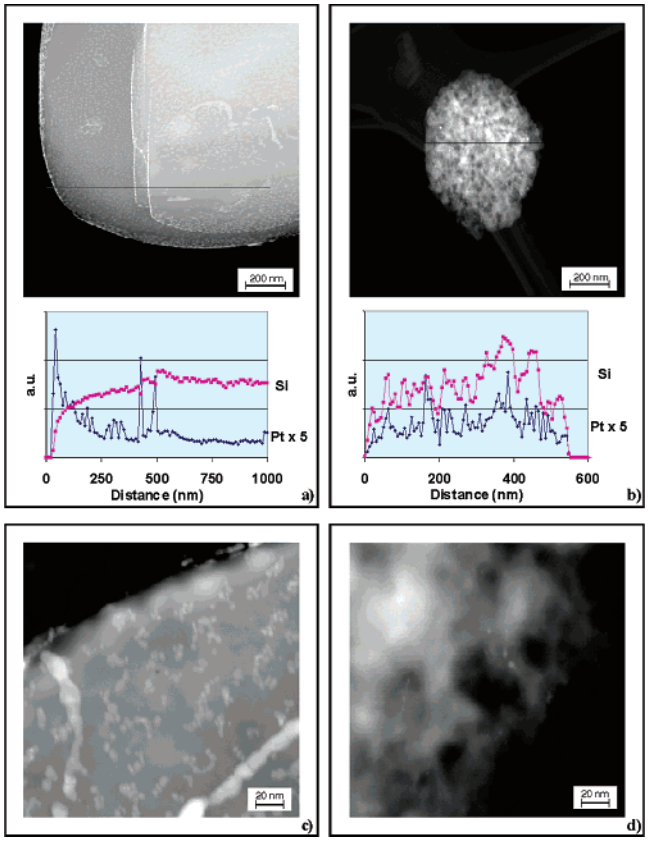

Figure 2. TEM images and EDS scans (Pt bottom and Si top) of Pt/conventional silicalite-1 (left column) and Pt/mesoporous silicalite-1 (right column) after calcination in air at 500 °C.

particle; note the significant increase in the Pt signal at the outer edges and twin edges (50, 320, 720, and 980 nm) where the beam direction is parallel to the edges. Several large Pt particles (ca. 30 nm) can be seen on the surface of the conventional zeolite sample in Figure 1 and other images taken during TEM investigation. The mesoporous silicalite-1 (Figure 1b,d) has a high intracrystalline porosity seen both directly in TEM and as fluctuations of the Si signal in EDS. In contrast to the Pt distribution on the surface of the conventional silicalite-1 particles, the Pt particles on the mesoporous silicalite-1 are well-dispersed throughout the entire mesopore system. As a consequence, the particle size of Pt is very small. From the line scan it can be seen that the Pt concentration is closely following the Si concentration, and large Pt particles were not detected. Thus, the presence of the mesopore system allows for a larger fraction of the zeolite volume to participate in dispersing the metal, resulting in smaller particle sizes in the mesoporous zeolite. The reason for this is most likely the high amount of lattice terminations along the mesopore system, which gives a high amount of lattice defects available for the crystallization of Pt.

Pt/Silicalite-1 Samples after Calcination at 500 °C. Many catalytic processes of industrial relevance involving Pt catalysts are carried out at elevated temperatures. An important parameter for the performance of the catalysts is the stability of the metal particles against sintering. To investigate the effect of a thermal treatment on metal dispersion, both Pt/silicalite-1 samples were subjected to calcination at 500 °C. TEM images (Figure 2) of the calcined conventional silicalite-1 sample show the expected increase of the Pt particle size. The sintering procedure led to a formation of Pt particle "islands" on the surface of the conventional silicalite-1. In the line scan it is clearly seen that Pt atoms are aggregated, most likely at defects and steps on the outer surface. In the calcined mesoporous silicalite-1 sample, only a few large Pt particles were detected. A random distribution of the Pt particles throughout the carrier was kept after the calcination.

PtSn/Silicalite-1. Alloy catalysts are another interesting group of catalysts, due to the bifunctional nature of the active phase. Best known are probably Pt−Re, Pt−Ir, and Pt−Sn, which are used for reforming of naphtha in refineries or the "three-way catalyst" containing alloys of Pt metals for treatment of engine exhausts gases.[25] Alloy catalysts are also attracting increasing academic attention for different reactions, one example being NiAu for steam reforming.[26] PtSn/silicalite-1 is an example of an alloy catalyst, which is currently being regarded for reactions such as hydrogenation/dehydrogenation reactions.[27] The presence of Sn decreases the size of Pt ensembles and thus reduces hydrogenolysis.

Again, two samples where prepared using either conventional or mesoporous silicalite-1 as support. Analysis of the PtSn/silicalite-1 samples showed that the metal loadings of the two samples are similar: 1.5 wt % Pt and 0.7 wt % Sn in the conventional silicalite-1 and 1.3 wt % Pt and 1.1 wt % Sn in the mesoporous silicalite-1. From EDS element mapping in the TEM of selected crystals it can be seen that the Pt and Sn are

(25) Olivas, A.; Jerdev, D. I.; Koel, B. E. *J. Catal.* **2004**, *222*, 285.
(26) Ponec, V. *Appl. Catal. A* **2001**, *2001*, 31.
(27) Besenbacher, F.; Chorkendorff, I.; Clausen, B. S.; Hammer, B.; Molenbroek, A. M.; Nørskov, J. K.; Stensgaard, I. *Science* **1998**, *279*, 1913.

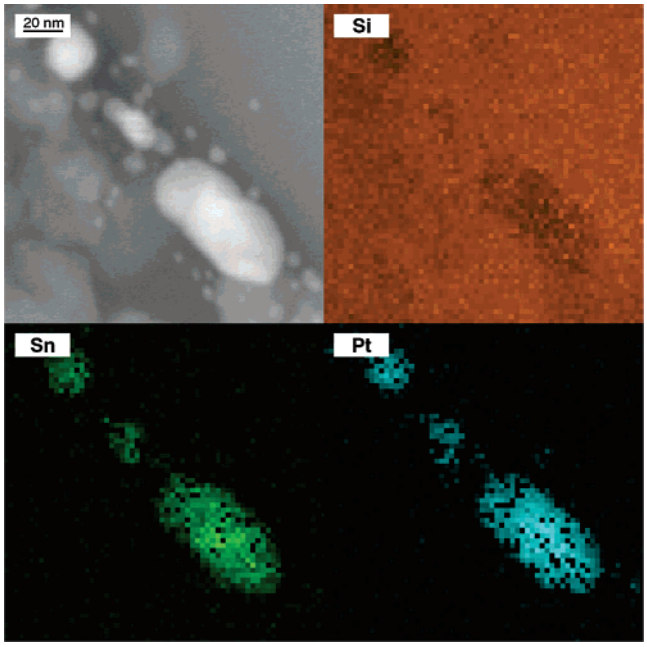

Figure 3. TEM image and element map of PtSn/conventional silicalite-1 particles. The element map is showing the local EDS signals of Si, Sn and Pt, respectively.

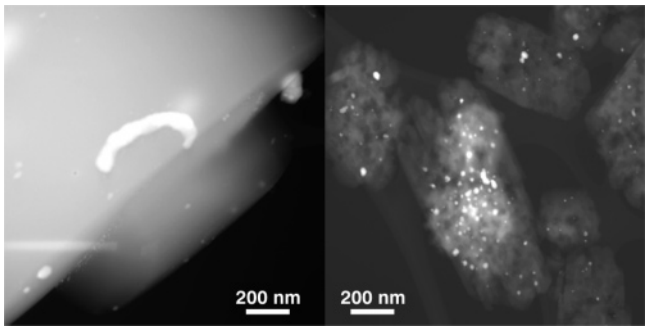

Figure 4. TEM images of PtSn/conventional silicalite-1 (left) and PtSn/mesoporous silicalite-1 (right) after calcination and reduction.

located in the same metal clusters at the same relative amounts throughout all clusters examined (Figure 3 and other images). This was seen for both samples. These element mappings thus indicate that Pt and Sn in both samples are alloyed and not two segregated metallic phases.

The TEM images of the two PtSn/silicalite-1 samples show the same trends as were seen with the Pt/silicalite-1 samples above: On the sample with conventional silicalite-1, the PtSn particles are located at the outer surface as a mixture of small particles (<10 nm) and large agglomerates (>100 nm). On the sample with mesoporous silicalite-1, PtSn is distributed throughout the zeolite crystal as small (<20 nm) particles, and no large particle agglomerates can be detected (Figure 4).

Thus, once more it has been shown that the mesoporous silicalite-1 sample allows the metals to disperse throughout the zeolite single crystal mesopore system as nanocrystals, whereas the use of a conventional silicalite-1 as support for PtSn gives a mixture of nanocrystals and large agglomerates that most likely are all located on the outer surface.

***β*-Mo_2C/ZSM-5.** Zeolite-supported β-Mo_2C is an example of a catalyst that is not metallic in nature. It is currently being investigated as a catalyst for methane dehydroaromatization. One

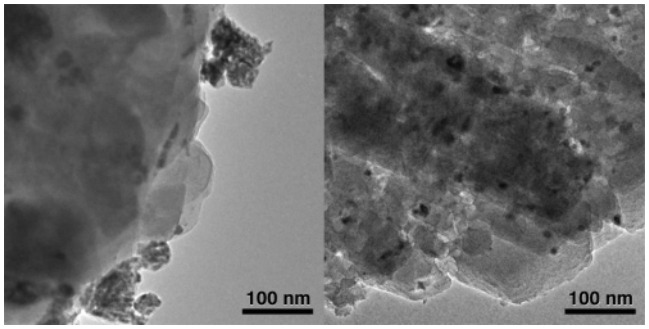

Figure 5. Bright field TEM images of β-Mo_2C/conventional ZSM-5 (left) and β-Mo_2C/mesoporous ZSM-5 (right), both after thermal treatment at 700 °C.

of the problems with this catalyst is the difficult preparation. It has to be carbonized at high temperatures, causing phase transformations and sintering, which lower the surface area of the β-Mo_2C phase.

XRPD confirmed the presence and purity of the β-Mo_2C phase after the preparation. No trace of MoO_3 was seen. The Mo loadings were 10.6 and 10.2 wt % on mesoporous and conventional zeolite ZSM-5, respectively.

The same trends are seen for the two samples of supported nonmetallic β-Mo_2C as with metallic Pt and PtSn. In the sample with conventional zeolite, the β-Mo_2C crystal agglomerates are of 100 nm size and located at the outer surface of the zeolite crystals, whereas using mesoporous zeolite single crystals the β-Mo_2C crystals are dispersed in the mesopore system with a size of <20 nm, even though both samples were prepared at 700 °C (Figure 5).

Conclusions

For several different examples of nanocrystals, i.e., pure metals, alloys, and carbides, deposited onto conventional zeolite crystals, our detailed TEM investigations show that the nanocrystals decorate the external surface of the zeolite. Additionally, the nanocrystals are clearly seen to preferentially deposit at defect sites at the surface. Thus, to obtain high concentrations of well-dispersed nanocrystals at zeolite surfaces, a high density of defect sites is required. This provides a new guideline for design of zeolite catalysts. With our recently discovered family of mesoporous zeolite single crystals, which are among the most porous materials known, the difficulty of site separation in bifunctional zeolite catalysts can be overcome. In this case, introduction of the nanocrystals is conveniently performed even at high concentrations, since the extensive mesopore system present in each crystal allows introduction of substantial amounts of precursor solutions. Upon transformation of the precursors into nanocrystals, the mesoporous zeolite single crystals provide a sufficient number of defect sites throughout the entire zeolite crystal to efficiently disperse nanocrystals in very close proximity to all the active sites in the micropores that are responsible for shape selectivity. In these materials, access to the nanocrystals is possible through both the micropores and the mesopores, and such materials show significant promise as heterogeneous catalysts. Accordingly, with the present methodology it is possible to distribute nanocrystals inside mesoporous zeolite single crystals.

JA050380U